JCB Journal of Cell Biology

REPORT

Mitochondrial fragmentation enables localized signaling required for cell repair

Adam Horn[1], Shreya Raavicharla[1], Sonna Shah[1], Dan Cox[2], and Jyoti K. Jaiswal[1,3]

Plasma membrane injury can cause lethal influx of calcium, but cells survive by mounting a polarized repair response targeted to the wound site. Mitochondrial signaling within seconds after injury enables this response. However, as mitochondria are distributed throughout the cell in an interconnected network, it is unclear how they generate a spatially restricted signal to repair the plasma membrane wound. Here we show that calcium influx and Drp1-mediated, rapid mitochondrial fission at the injury site help polarize the repair response. Fission of injury-proximal mitochondria allows for greater amplitude and duration of calcium increase in these mitochondria, allowing them to generate local redox signaling required for plasma membrane repair. Drp1 knockout cells and patient cells lacking the Drp1 adaptor protein MiD49 fail to undergo injury-triggered mitochondrial fission, preventing polarized mitochondrial calcium increase and plasma membrane repair. Although mitochondrial fission is considered to be an indicator of cell damage and death, our findings identify that mitochondrial fission generates localized signaling required for cell survival.

Introduction

Plasma membrane (PM), the physical barrier that contains all of the cell's vital processes, is susceptible to injury. To successfully repair the PM, a cell must determine the location and size of the injury and mount a localized and coordinated repair response (Horn and Jaiswal, 2018). While our understanding of the machinery of plasma membrane repair (PMR) is growing, less is known about the origin and control of signals that localize and coordinate the repair response. Previously, we identified that mitochondria play a critical role in PMR by uptake of calcium entering the injured cell and generation of redox signaling to activate localized assembly of F-actin (Horn et al., 2017), a process known to help with the repair of PM injuries (DeKraker et al., 2019; Demonbreun et al., 2016; Horn et al., 2017; Jaiswal et al., 2014; McDade et al., 2014).

As the cell's energy hub, mitochondria receive metabolic signals from the cellular environment and respond by regulating ATP production. However, mitochondria can also produce signals that help maintain cellular homeostasis during growth and stress responses (Chandel, 2015). Mitochondria are distributed throughout the entire cell and behave as an interconnected network while simultaneously maintaining contact with other organelles (Glancy et al., 2015; Murley and Nunnari, 2016). This cell-wide distribution of mitochondria is conducive for responding to perturbations that require global responses such as increased energy production (Chandel, 2015; Mishra and Chan, 2014). However, it is unclear how this interconnected mitochondrial network could respond to local perturbations, such as focal PM damage, that require producing and maintaining localized signals (Horn et al., 2017).

Fusion and fission enable mitochondria to behave as isolated organelles or as an interconnected network (Mishra and Chan, 2014). These morphological changes are intimately related to mitochondrial function, including regulation of metabolism and signaling (Szabadkai et al., 2006; Westermann, 2012). Fusion of mitochondria is facilitated by Mitofusins 1 and 2 (Mfn1 and Mfn2), located at the outer mitochondrial membrane (OMM) and optic atrophy 1 (Opa1) at the inner mitochondrial membrane (Ban et al., 2017; Tilokani et al., 2018). In contrast, mitochondrial fission (fragmentation) is enabled by Dynamin-related protein 1 (Drp1). Drp1 adaptor proteins such as mitochondrial dynamics protein 49 (MiD49), MiD51, mitochondrial fission 1, and mitochondrial fission factor are located on the OMM and help recruit Drp1 to mitochondria (Kraus and Ryan, 2017; Pagliuso et al., 2018; Tilokani et al., 2018). During stress, mitochondrial fusion increases connectivity and functional efficiency of the network, while fragmentation helps remove damaged mitochondria and is

[1]Children's National Health System, Center for Genetic Medicine Research, Washington, DC; [2]John Walton Muscular Dystrophy Research Centre, Newcastle University and Newcastle Hospitals National Health Service Foundation Trust, Newcastle upon Tyne, UK; [3]Department of Genomics and Precision Medicine, George Washington University School of Medicine and Health Sciences, Washington, DC.

Correspondence to Jyoti K. Jaiswal: jkjaiswal@cnmc.org.

associated with cell death and degeneration (Bossy-Wetzel et al., 2003; Brooks et al., 2007; Frank et al., 2001; Youle and van der Bliek, 2012).

Mitochondria help repair and regenerate cells following PM injury, and defects in this process result in degenerative disease (Boehler et al., 2019; Debattisti et al., 2019; Han et al., 2016; Horn et al., 2017; Sharma et al., 2012; Vila et al., 2017; Xu and Chisholm, 2014). PM injury in neurons and skeletal myofibers leads to mitochondrial traffic to the injury site, but even in cell types where mitochondria do not traffic to the injury site, mitochondrial signaling is required for repair (Cheng et al., 2015; Han et al., 2016; Horn et al., 2017; Sharma et al., 2012; Vila et al., 2017; Xu and Chisholm, 2014; Zhou et al., 2016). Here, we investigated how the mitochondrial network produces localized signaling to repair focal membrane injury. We found that injury triggers local fragmentation of the mitochondrial network at the injury site. The fragmented mitochondria then focally generate redox signaling that facilitates local polymerization of F-actin, which aids in wound closure. This process is disrupted in cells lacking Drp1 and in patient cells lacking a Drp1 receptor protein, MiD49, both of which prevent mitochondrial fragmentation. This identifies a new role for mitochondrial fragmentation in mediating acute and focal signaling, which is necessary for cell survival.

Results and discussion

To assess the mitochondrial network response to PM injury, we monitored mitochondria in WT primary mouse embryonic fibroblasts (MEFs) following focal PM injury. Within a few seconds after injury, mitochondria proximal to the injury site fragmented away from the network (Fig. 1 A and Video 1). This continued for 30 s after injury but did not involve distal mitochondria. Mitochondria in nearly one third of the cell area proximal to the injury site responded by retracting away from the injury site (Fig. 1 B, dotted box) and 25.8 ± 3.8% of these responsive mitochondria fragmented following injury. Similar to focal laser injury, mechanical injury by glass beads also caused the mitochondria at the site of injury to fragment (Fig. S1 A).

Because of the general association of mitochondrial fragmentation with cell damage, mitochondrial dysfunction, and apoptosis, we hypothesized that the observed mitochondrial fragmentation during the first 30 s of PMR was indicative of injury-induced mitochondrial damage. To test this, we asked whether inhibiting membrane repair increases mitochondrial fragmentation. As cytosolic calcium ($[Ca^{2+}]_c$) increase by the entry of extracellular calcium is required for PMR (Steinhardt et al., 1994), we inhibited PMR by depleting extracellular calcium. To monitor PMR, we used membrane-impermeable dye, FM 1-43, which increases in fluorescence upon entering the cell. Successful PMR closes the wound and prevents continued increase in dye fluorescence, causing it to plateau, while PMR failure is evident by unabated dye uptake (Fig. 1 C). Injury in the absence of extracellular calcium prevented most (87.3 ± 6.39%) of the injured cells from repairing (Fig. 1 D). Failed PMR due to the absence of Ca^{2+} reduced (not increased) mitochondrial fragmentation by 50-fold (0.49 ± 0.24% fragmentation compared with 25.8 ± 3.8%; Fig. 1 E). These results indicated that mitochondrial fragmentation is not just an outcome of PM damage, but rather, is part of a Ca^{2+}-triggered repair response.

We previously identified that injury-triggered mitochondrial calcium ($[Ca^{2+}]_m$) uptake is needed for PMR (Horn et al., 2017). $[Ca^{2+}]_m$ overload can depolarize mitochondria, leading to their fragmentation (Cereghetti et al., 2008; Duchen et al., 1998). We have described that $[Ca^{2+}]_m$ increases within seconds of PM injury and returns to baseline within the next minute as the cell repairs (Horn et al., 2017). We investigated if this $[Ca^{2+}]_m$ uptake affects mitochondrial membrane potential after injury and found that, similar to Ca^{2+} increase, injury proximal (but not distal) mitochondria immediately depolarized and did so before fragmentation (Fig. 1, F–H). This suggested that Ca^{2+} uptake may drive mitochondrial fragmentation through mitochondrial depolarization and mitochondrial reactive oxygen species (mROS) production. Using drugs that we previously found to inhibit injury-triggered $[Ca^{2+}]_m$ uptake (ruthenium red) and mROS production (mitoTEMPO), we found that, unlike blocking extracellular Ca^{2+} entry (Fig. 1 E), preventing increased $[Ca^{2+}]_m$ or mROS did not prevent mitochondrial fragmentation (Fig. 1, I and J). Depolarization of mitochondria was transient, as they repolarized within a minute after injury (Fig. 1, G and H), with a time course concomitant with the return of $[Ca^{2+}]_m$ to preinjury baseline (Horn et al., 2017). Despite being repolarized, these mitochondria remained isolated from the rest of the network, indicating that mitochondrial function is restored to the preinjury state independently of their integration into the mitochondrial network. These results identify that injury triggers mitochondrial fragmentation by increase in $[Ca^{2+}]_c$, independent of increase in $[Ca^{2+}]_m$, mROS, or depolarization.

Next, we manipulated mitochondrial shape without simultaneously inhibiting calcium-dependent repair pathways by using fibroblasts from Mfn1 and Mfn2 double-knockout (DKO) mice (MFN DKO). Absence of the Mfns prevents mitochondrial fusion and disassembles the mitochondrial network due to unchecked mitochondrial fragmentation (Chen et al., 2005). We confirmed that mitochondria in MFN DKO cells were completely fragmented even before PM injury, and we observed no further fragmentation following focal injury (Fig. 2 A). However, these cells underwent efficient PMR, causing the kinetics of FM 1-43 dye uptake and the proportion of cells that failed to repair to be similar to the WT cells (Fig. 2, B and C). To ensure that the prefragmented mitochondria in MFN DKO cells supported the local signaling needed for successful PMR, we assessed F-actin accumulation at the repair site, the downstream effect of localized mitochondrial signaling. F-actin accumulated with the same kinetics and amplitude as the WT MEFs (Fig. 2, D and E), identifying that mitochondrial fragmentation is supportive, not detrimental, for PMR.

In contrast to lack of mitochondrial fusion resulting in a fragmented mitochondrial network, lack of mitochondrial fission results in a hyperelongated mitochondrial network described in cells lacking the Drp1 adaptor protein MiD49 (Bartsakoulia et al., 2018; Palmer et al., 2011). Patients lacking MiD49 suffer from a neuromuscular disease characterized by high serum creatine kinase levels and presence of degenerated

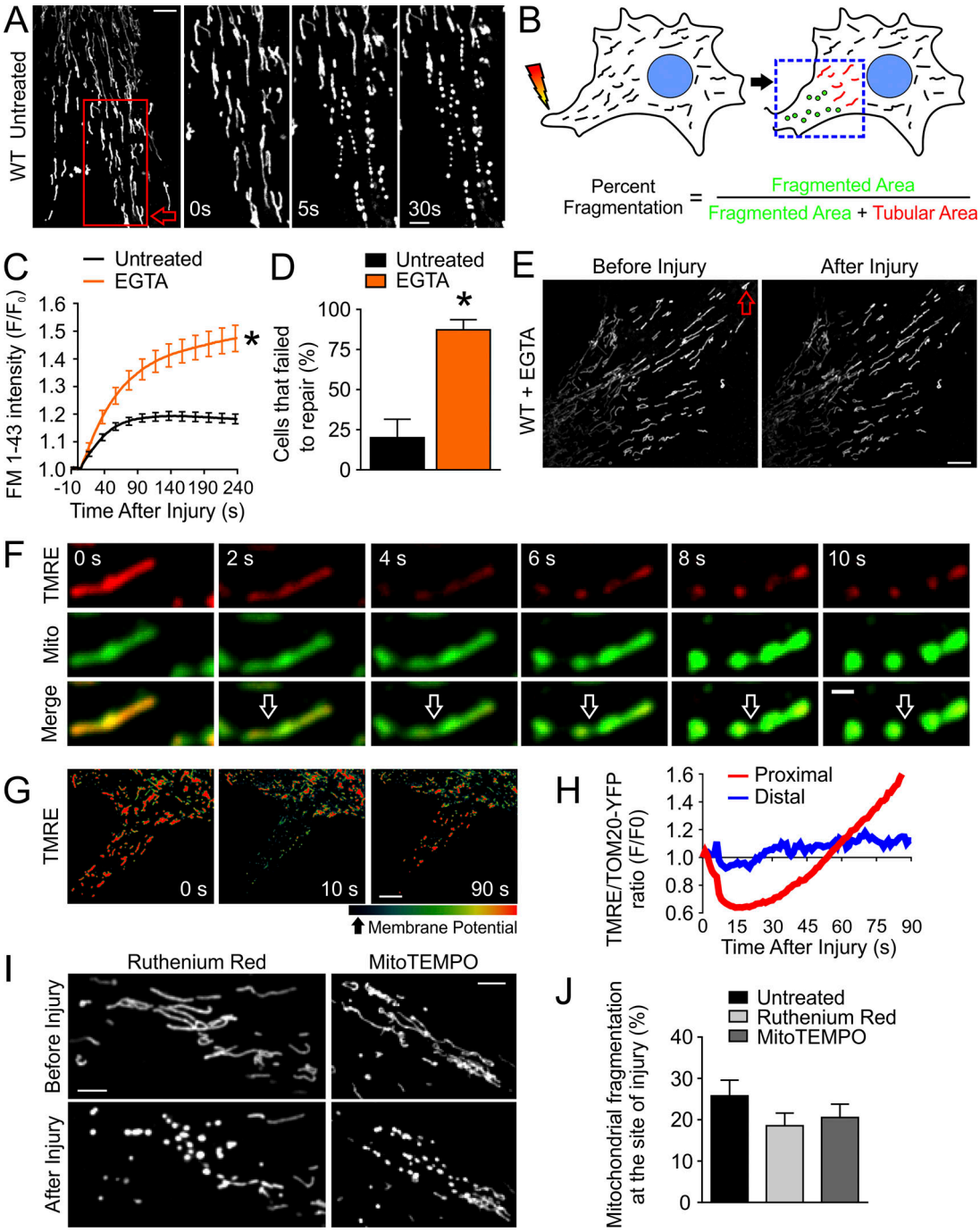

Figure 1. **Rapid and localized mitochondrial fragmentation occurs in response to PM injury. (A)** WT MEF showing mitochondria labeled with MitoTracker Green before and after PM injury. Red box indicates the area magnified on the right. **(B)** Schematic showing mitochondrial fragmentation analysis. Cells were injured by pulsed laser (left); dotted box (right) marks the mitochondria that responded in the injured cell. Extent of fragmentation 30 s after injury was calculated by dividing the area of injured cells with fragmented (green) mitochondria by the area of cells containing the responding mitochondria (dotted box). **(C)** FM 1-43 dye intensity after injury of untreated (n = 17) or EGTA-treated (n = 21) WT MEFs. **(D)** Percentage of cells that failed to repair (n = 3 experiments). **(E)** Images showing mitochondrial shape in response to PM injury in EGTA-treated WT MEFs. **(F)** Images showing injury-induced change in mitochondrial membrane potential in a mitochondrion labeled with TMRE and TOM20-YFP (Mito). Arrows indicate sites of fragmentation. **(G)** Heat map images showing change in TMRE fluorescence intensity after injury. **(H)** Plot showing the ratio of TMRE/TOM20-YFP fluorescence intensity of cell shown in G. **(I)** Images showing shape of injury-proximal mitochondria during PMR in WT MEFs treated with ruthenium red or mitoTEMPO. **(J)** Extent of mitochondrial fragmentation at injury site (n = 3 experiments). Unless otherwise noted, arrows mark the site of injury. Scale bar = 10 µm (A, E, and G) or 5 µm (A inset and I) or 1 µm (F). *, $P < 0.05$ by unpaired t test. Error bars represent SEM.

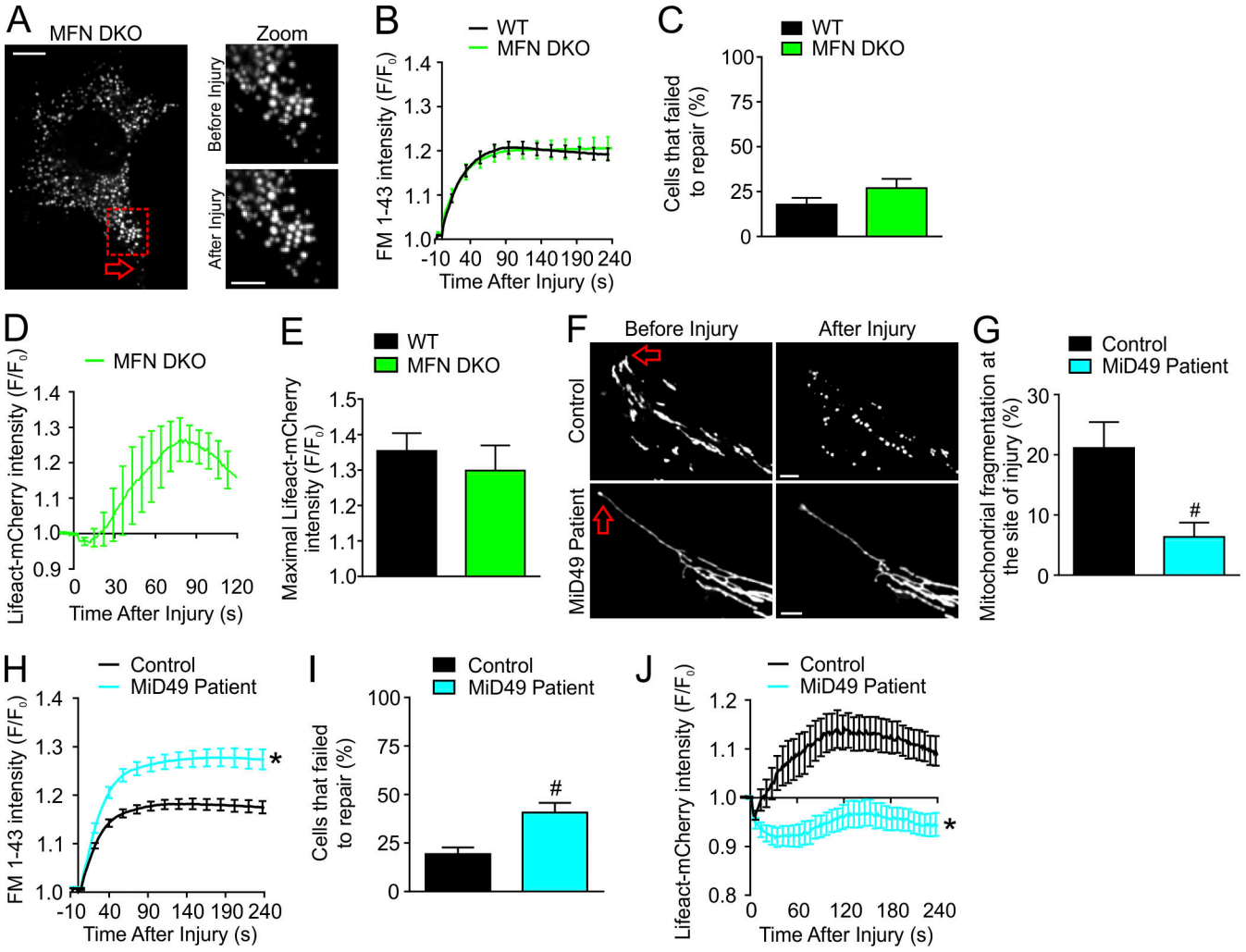

Figure 2. **Mitochondrial fragmentation is required for PMR. (A)** Images showing mitochondrial shape before and after PM injury in MFN DKO MEFs. Dotted red box marks the magnified region on the right. **(B)** FM 1-43 dye intensity after injury to WT (n = 56) and MFN DKO MEFs (n = 37). **(C)** Percentage of cells that failed to repair in independent experiments (n = 6 experiments). **(D)** Kinetics of Lifeact-mCherry at injury site in MFN DKO MEFs (n = 4). **(E)** Maximal Lifeact-mCherry intensity after injury in WT (n = 3) and MFN DKO (n = 4) MEFs. **(F)** Images showing mitochondria near the site of PM injury in healthy control and MiD49 patient fibroblasts. **(G)** Plot quantifying mitochondrial fragmentation after injury in control (n = 21) and MiD49 patient fibroblasts (n = 28 cells). **(H)** FM 1-43 dye intensity after injury in control (n = 50) and MiD49 patient fibroblasts (n = 48 cells). **(I)** Percentage of cells that failed to repair (n = 5 experiments). **(J)** Lifeact-mCherry intensity after PM injury in control and MiD49 patient fibroblasts (n = 13 control and 19 MiD49 patient cells). Mitochondria are marked by MitoTracker Green. Arrows mark the site of injury. Scale bar = 10 µm (whole cell, A) and 5 µm (zoom, A and F). *, P < 0.05 by unpaired t test. #, P < 0.05 by Mann–Whitney U test. Error bars represent SEM.

myofibers (Bartsakoulia et al., 2018). These are signs of muscle damage common in muscle diseases associated with poor PMR (Defour et al., 2017; Vila et al., 2017; Wu and Perryman, 1992), which suggests that reduced mitochondrial fission in the MiD49-deficient patients may cause poor muscle cell PMR. We confirmed that MiD49-deficient patient cells exhibit a hyperelongated mitochondrial network (Fig. S1 B). Upon focal membrane injury, 21.1 ± 4.3% of injury-proximal mitochondria fragmented in healthy donor cells, which was reduced to 6.3 ± 2.4% in the patient cells (Fig. 2, F and G; Videos 2 and 3). This reduction in injury-triggered mitochondrial fragmentation correlated with poor PMR of these patient cells (Fig. 2 H). Compared with 19.3 ± 3.4% of healthy cells, 40.7 ± 4.9% of patient cells failed to repair (Fig. 2 I). In contrast to the robust accumulation of F-actin in control cells, F-actin failed to accumulate following injury in MiD49 patient cells (Fig. 2 J). These results indicate that injury-triggered mitochondrial fragmentation is a facilitator of the PMR response.

MiD49, along with other adaptor proteins, recruits Drp1 to mitochondria to enable fragmentation (Kamerkar et al., 2018; Kraus and Ryan, 2017). Therefore, we examined whether Drp1 is recruited to mitochondria following injury. PM injury induced a rapid and localized accumulation of Drp1 on the injury-proximal mitochondria (Fig. 3 A and Video 4). To test if Drp1-mediated mitochondrial fragmentation is required for PMR, we used MEFs with targeted Drp1 deletion (DRP1 KO; Salka et al., 2017; Wakabayashi et al., 2009). These cells have a highly connected mitochondrial network (Fig. S1 C) and, upon injury, showed 10-fold lower injury-triggered mitochondrial fragmentation (Fig. 3, B and C; and Video 5). This reduction in mitochondrial

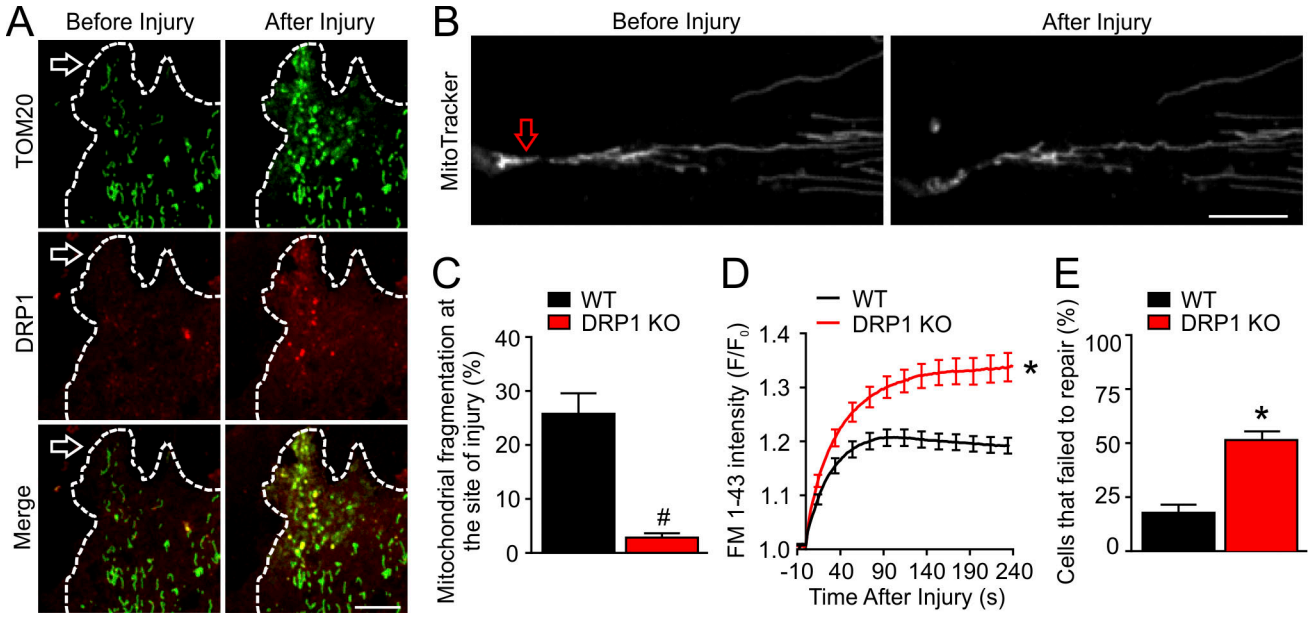

Figure 3. **DRP1 facilitates injury-triggered mitochondrial fragmentation. (A)** DRP1 recruitment to mitochondria in response to PM injury. Mitochondria are labeled by OMM protein TOM20, and dotted line indicates cell boundary. **(B)** Response of MitoTracker Green–labeled mitochondria (arrow) in DRP1 KO MEFs to PM injury. **(C)** Plot quantifying mitochondrial fragmentation after injury in WT (n = 16 cells) DRP1 KO cells (n = 27 cells). **(D)** FM 1-43 dye intensity after injury of WT (n = 56 cells) and DRP1 KO MEFs (n = 43 cells). **(E)** Plot showing percentage of cells that failed to repair (n = 6 experiments). Arrows mark the site of injury. Scale bar = 10 µm (A) and 5 µm (B). *, P < 0.05 by unpaired t test. #, P < 0.05 by Mann–Whitney U test. Error bars represent SEM.

fragmentation was coincident with excessive FM dye uptake and reduced ability of DRP1 KO MEFs to repair (Fig. 3, D and E). To determine if poor PMR is also a feature of Drp1-deficient human cells, we monitored injury-triggered mitochondrial fragmentation in Drp1 KO HeLa cells (Otera et al., 2016). Similar to the MEFs, Drp1 and extracellular calcium were also required for injury-triggered mitochondrial fragmentation in the HeLa cells (Fig. S2, A–C), and lack of Drp1 compromised F-actin accumulation and PMR in these human cells (Fig. S2, D–F).

Injury-triggered $[Ca^{2+}]_m$ increase causes mROS signaling required for F-actin polymerization at the site of damage (Horn et al., 2017). Therefore, we used the mitochondria-localized calcium sensor mCAR-GECO1 (Wu et al., 2013) to test whether Drp1 deficit affects $[Ca^{2+}]_m$ dynamics following injury. Injury to WT MEFs caused a rapid increase in $[Ca^{2+}]_m$ throughout the cell; however, this increase was both higher and slower to return to baseline in the injury-proximal (fragmented) mitochondria compared with the distal (tubular) mitochondria (Fig. 4, A and D). Lack of Drp1 abrogated the differences in amplitude and kinetics of $[Ca^{2+}]_m$ uptake between injury-proximal and -distal mitochondria (Fig. 4, B and D). While the $[Ca^{2+}]_m$ in the injury-proximal mitochondria increased by 2.9-fold in WT cells, this increased to only 1.7-fold in DRP1 KO cells (Fig. 4 E). Further, $[Ca^{2+}]_m$ in the injury-proximal mitochondria returned to half its maximum value twice as fast in the DRP1 KO MEFs compared with the WT MEFs (Fig. 4 F). Areas under the curve for mCAR-GECO1 intensity traces showed fivefold lower $[Ca^{2+}]_m$ load in injury-proximal mitochondria in DRP1 KO MEFs (59.6 ± 9.6) compared with WT MEFs (255.9 ± 46.6). Measurement of $[Ca^{2+}]_m$ throughout the whole cell (including distal mitochondria) showed that DRP1 KO MEFs took up significantly less Ca^{2+} overall, but that kinetics of Ca^{2+} increase were unchanged (Fig. S3, A–E). These findings show that failure of injury-proximal mitochondria to fragment significantly reduces local injury-triggered Ca^{2+} increase. To further test the effect of fragmented mitochondria on $[Ca^{2+}]_m$ uptake after injury, we next examined MFN DKO cells. These cells showed no difference from WT MEFs in polarization of $[Ca^{2+}]_m$ increase (higher in injury-proximal versus injury-distal mitochondria), the amplitude of $[Ca^{2+}]_m$ uptake, and the time for $[Ca^{2+}]_m$ to return to its half-maximal value (Fig. 4, C–F). Given this, we asked whether lack of injury-triggered mitochondrial fragmentation observed in MiD49-deficient patient cells would produce a $[Ca^{2+}]_m$ response similar to DRP1 KO MEFs. Similar to DRP1 KO MEFs, MiD49-deficienct cells lacked differential $[Ca^{2+}]_m$ uptake between injury-proximal and -distal mitochondria and trended toward a reduced uptake and retention of Ca^{2+} in injury-proximal mitochondria (Fig. S3, F–H). Together, the results above show that fragmented mitochondria at the injury site are essential for polarized $[Ca^{2+}]_m$ homeostasis following injury.

Increase in $[Ca^{2+}]_m$ promotes mROS production (Brookes et al., 2004), which enables PMR by Ras homology family member A (RhoA)-dependent F-actin accumulation at the wound site (Horn et al., 2017). With mitochondrial fragmentation enhancing the $[Ca^{2+}]_m$ response in the injury-proximal mitochondria, we examined if this process regulates polarized redox signaling during PMR. Direct visualization of active RhoA using the Forster resonance energy transfer (FRET)-based biosensor RhoA-FLARE confirmed selective activation of RhoA in the injury-proximal region (Fig. 5 A). Similarly, production of local mROS and local F-actin accumulation, which are required for PMR, were also high in the injury-proximal regions

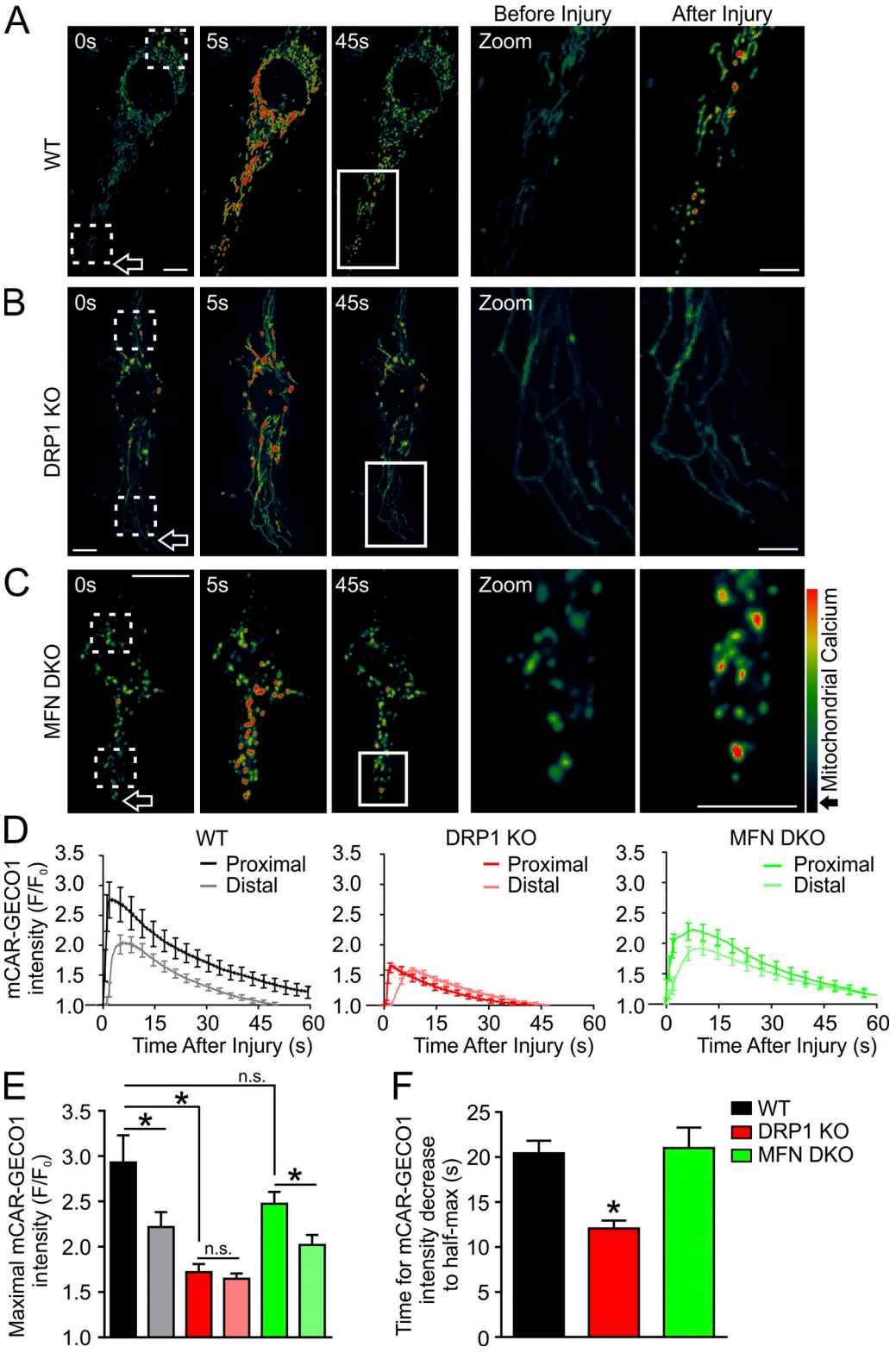

Figure 4. **Fragmented mitochondria sustain high mitochondrial calcium levels at the injury site. (A–C)** Time series of mitochondrial calcium uptake (mCAR-GECO1) in WT (A), DRP1 KO (B), and MFN DKO (C) MEFs after PM injury. Dotted boxes illustrate representative injury proximal and injury distal regions used for measurements. Solid box indicates magnified area at right. Arrow marks the site of injury. Scale bar = 10 µm (whole cell) and 5 µm (zoom). **(D)** mCAR-GECO1 intensity after PM injury (n = 12 WT, 16 DRP1 KO, and 16 MFN DKO cells). **(E)** Maximal $[Ca^{2+}]_m$ uptake in injury-proximal and injury-distal mitochondria (n = 12 WT, 16 DRP1 KO, and 16 MFN DKO cells). **(F)** Time for $[Ca^{2+}]_m$ to decrease to half peak (n = 12 WT, 16 DRP1 KO, and 16 MFN DKO cells). *, $P < 0.05$ by unpaired t test; n.s., not significant. Error bars represent SEM.

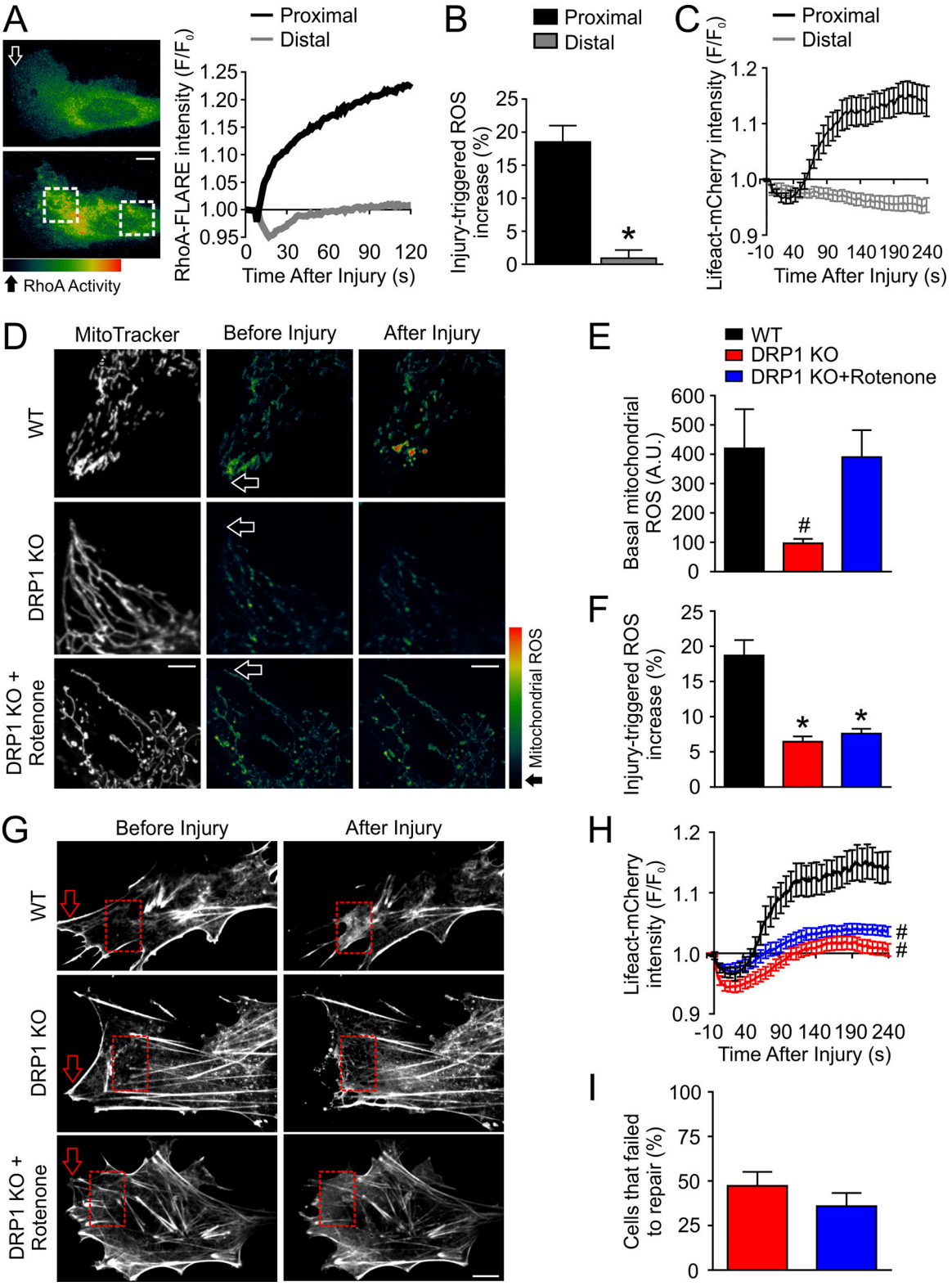

Figure 5. **Mitochondrial fragmentation is required for redox signaling during repair. (A)** RhoA activity (RhoA-FLARE) in an injured WT MEF. **(B)** Plot showing mROS (MitoSOX) increase in response to PM injury in WT MEFs (n = 12 cells). **(C)** Lifeact-mCherry kinetics after PM injury in WT MEFs (n = 12 cells). **(D)** Images of MEFs costained with MitoTracker Green (left) and MitoSOX Red (right). MitoSOX images are shown before and 30 s after PM injury. **(E)** Basal mitochondrial ROS level in the absence of injury (n = 16 WT, 20 untreated DRP1 KO, and 14 rotenone-treated DRP1 KO MEFs). **(F)** Mitochondrial ROS increase in response to PM injury (n = 12 WT, 18 untreated DRP1 KO, and 11 rotenone treated DRP1 KO cells). **(G)** F-actin (Lifeact-mCherry) response to PM injury. Dotted box indicates injury-proximal region used for quantification. **(H)** Change in Lifeact-mCherry intensity after PM injury in WT (n = 12), DRP1 KO (n = 46), and rotenone-treated DRP1 KO MEFs (n = 37 cells). **(I)** Percentage of untreated and rotenone-treated DRP1 KO cells that failed to repair (n = 5 experiments). Arrows mark the site of injury. Scale bar = 5 µm (D) and 10 µm (A and G). *, P < 0.05 by unpaired t test. #, P < 0.05 by Mann–Whitney U test. Error bars represent SEM.

(Fig. 5, B and C). To test whether lack of mitochondrial fragmentation prevents polarized PMR signaling, we quantified mROS in DRP1 KO cells and found that, compared with the WT MEFs, mROS levels were lower at baseline in DRP1 KO cells and were reduced by threefold following injury (6.45 ± 0.76% increase in DRP1 KO MEFs and 18.7 ± 2.18% in WT MEFs; Fig. 5, D–F). This deficit is not due to the inability of DRP1 KO mitochondria to produce ROS, as treatment with a known mROS agonist, rotenone (Li et al., 2003), increased basal mROS to a level comparable to WT MEFs (Fig. 5, D and E).

We next tested whether inefficient mROS production also affects F-actin dynamics during repair and found this to be the case in DRP1 KO MEFs and DRP1 KO HeLa cells (Fig. 5, G and H; and Fig. S2 F). As acute rotenone treatment of healthy cells enhances injury-induced ROS production and improves membrane repair (Horn et al., 2017), and rotenone increased basal ROS level in DRP1 KO cells (Fig. 5, D and E), we next assessed whether this would improve mROS production and increase F-actin accumulation in DRP1 KO cells. Rotenone did not enhance injury-proximal mROS production, nor did it improve local F-actin accumulation or the ability of DRP1 KO cells to repair (Fig. 5, D–I). This highlights the importance of mitochondrial fragmentation in the precise spatial and temporal control of mitochondrial signaling at the injury site. This also demonstrated that a global increase in $[Ca^{2+}]_m$ and mROS production cannot compensate for the lack of localized mROS production during repair.

Our work here adds to the role of mitochondria, extending it beyond bioenergetics and metabolism to being a signaling hub for regulating cellular and organismal functions (Chandel, 2015; Yun and Finkel, 2014). Mitochondrial signaling is known to be mediated by the metabolic byproducts of mitochondrial reactions (Chandel, 2015; Chin et al., 2014; Katewa et al., 2014). mROS is one such byproduct that activates adaptive signaling and antioxidant gene expression at low levels (Hamanaka and Chandel, 2010; Yun and Finkel, 2014). However, high levels of ROS can cause irreversible damage to cellular components and lead to apoptosis (Hamanaka and Chandel, 2010). Therefore, tight control over the amount and timing of ROS production is critical for signaling. Previous studies have identified that repair of cell injury requires mitochondrial calcium uptake and redox signaling to facilitate RhoA-mediated F-actin polymerization (Cheng et al., 2015; Horn et al., 2017; Xu and Chisholm, 2014). Here, we show that extracellular calcium influx due to cell injury activates Drp1-mediated fragmentation of mitochondria at the site of injury. The fragmentation of mitochondria at the injury site enables modulation of the amplitude and duration of $[Ca^{2+}]_m$ increase, which in turn allows polarized mROS signaling at the wound site. Fragmentation of mitochondria during cell stress protects the mitochondrial network from calcium overload and apoptotic cell death (Szabadkai et al., 2006). We show that in the context of cell injury, mitochondrial fragmentation increases the Ca^{2+} load of injury-proximal mitochondria, which is disrupted by the lack of MiD49 or Drp1. Thus, the role of mitochondrial fragmentation extends beyond a protective effect to support localized signaling required for the survival of injured cells.

Failure to efficiently repair PM damage is associated with degenerative diseases affecting mechanically active tissues, such as skeletal muscle, that are exposed to frequent injury (Boehler et al., 2019; Vila et al., 2017). Recent studies in skeletal muscle have also demonstrated that postnatal dysregulation of mitochondrial fragmentation due to Drp1 KO (Favaro et al., 2019), or of mitochondrial calcium homeostasis due to MICU1 KO (Debattisti et al., 2019), results in progressive muscle wasting disorders similar to those caused by the inability of myofibers to repair PM damage (Bansal et al., 2003; Defour et al., 2017; Vila et al., 2017). While the calcium imbalance due to MICU1 deficit leads to poor myofiber repair (Debattisti et al., 2019), poor PMR has not been examined in Drp1-deficient mice. Our work here identifies MiD49 deficiency as another muscle disease in which failed PMR may contribute to pathogenesis. Our finding of poor PMR due to the lack of MiD49 provides an explanation for the observed exercise intolerance, signs of myofiber death, and resulting muscle weakness seen in patients (Bartsakoulia et al., 2018).

Although mitochondrial function is often viewed as a feature of the globally integrated mitochondrial network, fission and fusion enable mitochondria to maintain the ability to respond to highly localized cellular events. While mitochondrial fission is conventionally viewed as a detriment to cell health and is associated with cell damage and apoptosis, our work highlights the need for a more nuanced view of mitochondrial form and function even under conditions of cell stress and damage. Through rapid fission, mitochondria are able to act as signaling hubs, enabling cells to mount a polarized repair response to a focal PM injury. This opens an avenue for further exploration into additional roles for mitochondria in which highly localized cellular needs must be met through polarized mitochondrial signaling.

Materials and methods

Cell culture and reagents

MEFs and HeLa cells were routinely cultured in DMEM with Glutamax, high glucose, and 110 mg/L sodium pyruvate (Invitrogen) supplemented with 10% FBS (Hyclone, Thermo Fisher Scientific) and with 100 mg/ml penicillin and 100 mg/ml streptomycin (Invitrogen) at 37°C and 5% CO_2. MEFs knocked out for Drp1 (Wakabayashi et al., 2009) and Mfn 1/2 (Chen et al., 2005), as well as Drp1 KO HeLa cells (Otera et al., 2016) and MiD49 patient cells (Bartsakoulia et al., 2018), were cultured as previously described. MitoTracker Green (Thermo Fisher Scientific) was incubated with cells at a working concentration of 150 nM at 37°C for 15 min. Cells were transfected with the indicated plasmid using Lipofectamine 2000 (Life Technologies) per manufacturer's instructions. Expression was allowed for 18–24 h before imaging. EGTA, mitoTEMPO, and rotenone were purchased from Sigma-Aldrich. Ruthenium red was purchased from Santa Cruz Biotechnology. All pharmacological treatments, unless stated otherwise, were performed in Cellular Imaging Medium (CIM; HBSS with 10 mM Hepes and 2 mM Ca^{2+}, pH 7.4) at 37°C. All cells were injured in the presence of the indicated drug. The plasmids used in this study were obtained from

Addgene or were gifts from an investigator: Dr. Robert Campbell (University of Alberta, Alberta, Canada; CMV-mito-CAR-GECO1; Addgene plasmid 46022; Wu et al., 2013), Dr. Michael Davidson (Florida State University, Tallahassee, FL; mCherry-Lifeact; Addgene Plasmid 54491; Riedl et al., 2010), Dr. Gia Voeltz (University of Colorado Boulder, Boulder, CO; DRP1-mCherry; Addgene Plasmid 49152; Friedman et al., 2011), and Dr. Klaus Hahn (University of North Carolina at Chapel Hill, Chapel Hill, NC; pTriEx-RhoA FLARE; Addgene Plasmid 12150; Pertz et al., 2006).

PMR assay

The details of the laser injury assay are as previously described (Defour et al., 2014) and outlined as follows. Cells cultured on coverslips were transferred to CIM and placed in a stage-top incubator maintained at 37°C. For laser injury, a 1–2-µm^2 area was irradiated for 10 ms with a pulsed laser. For quantification of PM repair, cells were preincubated with the indicated treatment before 1 mg/ml FM 1-43 dye (Life Technologies) was added to CIM before injury. FM dye intensity (F/F_0, where F_0 represents baseline fluorescence) was used to calculate the kinetics of repair. Successful repair was determined by the entry of FM dye into the cell interior, where a plateau in FM dye increase indicated successful repair. Failure to repair was indicated by continued FM dye increase in cells out to 4 min after injury.

Glass bead injury was performed by rolling glass beads (Sigma-Aldrich) over cells cultured on coverslips as previously described (Defour et al., 2014). Cells were treated with MitoTracker Green as described above to label mitochondria and injured in the presence of lysine-fixable TRITC-dextran (2 mg/ml; Life Technologies) to mark injured cells. After injury, cells were allowed to heal at 37°C for 5 min, followed by fixation using 4% PFA.

Mitochondrial fragmentation analysis

Mitochondrial fragmentation was quantified using MetaMorph image analysis software (Molecular Devices). First, mitochondria responding to cell injury were identified by physical behavior, indicated by retraction after laser injury. Responding mitochondria, now defined as injury proximal, comprised less than one third of the total mitochondria in all cells. Integrated morphometry analysis was used to identify the total area of injury-proximal mitochondria before injury. 30 s after injury, the area of mitochondria that underwent fragmentation was quantified and used to calculate the percentage of injury-proximal mitochondria that fragmented in response to injury. A time gate of 30 s was chosen because of our observation that all WT cells had undergone fragmentation by this time after injury. Successful fragmentation was determined by the absence of fluorescence signal between two mitochondria that were previously present as one.

Quantification of mitochondrial membrane potential, calcium increase, and ROS production

Mitochondrial calcium was measured using the mitochondria-localized CAR-GECO1 calcium sensor. Cells were transfected with mito-CAR-GECO1 as described above, and fluorescence increase is presented as F/F_0. Calcium increase in mitochondria, both proximal and distal to the site of injury, was determined as described above. Mitochondrial membrane potential was assessed using tetramethylrhodamine ethyl ester (TMRE; Thermo Fisher Scientific). Change in membrane potential was quantified as the ratio of TMRE fluorescence to the fluorescence of mitochondrial structural marker TOM20-YFP. To detect mROS, cells were incubated in 2.5 µM MitoSOX (Thermo Fisher Scientific) for 15 min at 37°C. After washing with prewarmed CIM, cells were injured by pulsed laser as described above, and the change in fluorescence over the initial mitoSOX fluorescence (F/F_0) was quantified.

Quantification of RhoA activity and F-actin dynamics

To detect active RhoA, cells were transfected with the FRET-based RhoA-FLARE biosensor. Three-channel FRET imaging was performed by monitoring the donor (445-nm laser excitation), acceptor (515-nm laser excitation), and transfer (FRET) channels being imaged. To generate a corrected FRET image, the emission for each channel was corrected for bleed-through and used to measure corrected FRET (F_C = transfer − corrected acceptor − corrected donor). For measurement of actin dynamics, cells were transfected with the F-actin binding peptide Lifeact-mCherry. In each case, transfection was performed as described above, and fluorescence intensity is presented as F/F_0.

Microscopy and image acquisition

Cells were imaged using an inverted IX81 Olympus microscope (Olympus America) custom-equipped with a CSUX1 spinning disc confocal unit (Yokogawa Electric Corp.). Images were collected using a 60× objective (1.45 NA). Images were acquired using an Evolve 512 EMCCD (Photometrics) at 1 Hz. Image acquisition and laser injury was controlled using Slidebook 6.0 (Intelligent Imaging Innovations). Live imaging experiments were performed in a Tokai Hit microscopy stage-top ZILCS incubator (Tokai Hit Co.) maintained at 37°C. Cells were imaged in CIM. For laser injury, a 1–2-µm^2 area was irradiated for 10 ms with a pulsed laser (Ablate!; 3i Intelligent Imaging Innovations).

Statistical analysis

Image acquisition and analysis was performed using Slidebook 6.0. Statistical analysis was performed using Prism (GraphPad). Statistical outliers were removed using the ROUT method in Prism (Motulsky and Brown, 2006). For all kinetic trace data, individual time points were compared across all cells in a given treatment to determine significance by unpaired *t* test. For all data, the D'Agostino and Pearson omnibus normality test was performed before determining the appropriate statistical test. Unpaired *t* tests were used for all normally distributed data (indicated by *), and Mann–Whitney *U* tests were used for nonparametric data (indicated by #). All comparisons were two sided. In all cases, data not indicated as significant should be considered not statistically different unless otherwise stated. All data are presented as mean ± SEM, with $P < 0.05$ considered statistically significant. At least three independent experiments were performed for all data shown. Images are representative of ≥10 cells observed in each case.

Online supplemental material

Fig. S1 shows mitochondrial morphology after injury and genetic KO of fission regulators MiD49 and Drp1. Fig. S2 shows that injury-triggered mitochondrial fragmentation is conserved in HeLa cells. Fig. S3 shows mitochondrial calcium uptake after PM injury in DRP1 KO and MiD49 patient cells. Video 1 shows that PM injury causes rapid fragmentation of mitochondria. Video 2 shows injury-triggered mitochondrial fragmentation in a healthy human fibroblast. Video 3 shows that MiD49 is required for injury-triggered mitochondrial fragmentation. Video 4 shows Drp1 recruitment to injury-proximal mitochondria following PM injury. Video 5 shows that Drp1 is required for injury-triggered mitochondrial fragmentation

Acknowledgments

Part of the work presented here is reported in the PhD dissertation of A. Horn. We thank Dr. Hiromi Sesaki (Johns Hopkins University, Baltimore, MD) for Drp1 KO MEFs, Dr. David Chan (California Institute of Technology, Pasadena, CA) for Mfn 1/2 DKO MEFs, and Dr. Katsuyoshi Mihara (Kyushu University, Fukuoka, Japan) for Drp1 KO HeLa cells; and Dr. Volker Straub (Newcastle University, Newcastle upon Tyne, UK) for help with MiD49 deficient patient cells. We thank the members of our laboratory for helpful comments and suggestions throughout the duration of this project.

A. Horn is supported by the National Institute of Arthritis and Musculoskeletal and Skin Diseases (T32ARO56993). J.K. Jaiswal acknowledges funding by grants from the National Institute of Arthritis and Musculoskeletal and Skin Diseases (R01AR055686) and the National Institute of Child Health and Human Development (U54HD090257).

The authors declare no competing financial interests.

Author contributions: A. Horn and J.K. Jaiswal designed the study. D. Cox generated the patient cells used. A. Horn performed all experiments with help from S. Raavicharla, S. Shah, and J.K. Jaiswal. A. Horn and J.K. Jaiswal wrote the paper.

Submitted: 26 September 2019
Revised: 5 February 2020
Accepted: 9 March 2020

References

Ban, T., T. Ishihara, H. Kohno, S. Saita, A. Ichimura, K. Maenaka, T. Oka, K. Mihara, and N. Ishihara. 2017. Molecular basis of selective mitochondrial fusion by heterotypic action between OPA1 and cardiolipin. *Nat. Cell Biol.* 19:856–863. https://doi.org/10.1038/ncb3560

Bansal, D., K. Miyake, S.S. Vogel, S. Groh, C.-C. Chen, R. Williamson, P.L. McNeil, and K.P. Campbell. 2003. Defective membrane repair in dysferlin-deficient muscular dystrophy. *Nature.* 423:168–172. https://doi.org/10.1038/nature01573

Bartsakoulia, M., A. Pyle, D. Troncoso-Chandía, J. Vial-Brizzi, M.V. Paz-Fiblas, J. Duff, H. Griffin, V. Boczonadi, H. Lochmüller, S. Kleinle, et al. 2018. A novel mechanism causing imbalance of mitochondrial fusion and fission in human myopathies. *Hum. Mol. Genet.* 27:1186–1195. https://doi.org/10.1093/hmg/ddy033

Boehler, J.F., A. Horn, J.S. Novak, N. Li, S. Ghimbovschi, I.E. Lundberg, H. Alexanderson, L. Alemo Munters, J.K. Jaiswal, and K. Nagaraju. 2019. Mitochondrial dysfunction and role of harakiri in the pathogenesis of myositis. *J. Pathol.* 249:215–226. https://doi.org/10.1002/path.5309

Bossy-Wetzel, E., M.J. Barsoum, A. Godzik, R. Schwarzenbacher, and S.A. Lipton. 2003. Mitochondrial fission in apoptosis, neurodegeneration and aging. *Curr. Opin. Cell Biol.* 15:706–716. https://doi.org/10.1016/j.ceb.2003.10.015

Brookes, P.S., Y. Yoon, J.L. Robotham, M.W. Anders, and S.-S. Sheu. 2004. Calcium, ATP, and ROS: a mitochondrial love-hate triangle. *Am. J. Physiol. Cell Physiol.* 287:C817–C833. https://doi.org/10.1152/ajpcell.00139.2004

Brooks, C., Q. Wei, L. Feng, G. Dong, Y. Tao, L. Mei, Z.-J. Xie, and Z. Dong. 2007. Bak regulates mitochondrial morphology and pathology during apoptosis by interacting with mitofusins. *Proc. Natl. Acad. Sci. USA.* 104:11649–11654. https://doi.org/10.1073/pnas.0703976104

Cereghetti, G.M., A. Stangherlin, O. Martins de Brito, C.R. Chang, C. Blackstone, P. Bernardi, and L. Scorrano. 2008. Dephosphorylation by calcineurin regulates translocation of Drp1 to mitochondria. *Proc. Natl. Acad. Sci. USA.* 105:15803–15808. https://doi.org/10.1073/pnas.0808249105

Chandel, N.S. 2015. Evolution of mitochondria as signaling organelles. *Cell Metab.* 22:204–206. https://doi.org/10.1016/j.cmet.2015.05.013

Chen, H., A. Chomyn, and D.C. Chan. 2005. Disruption of fusion results in mitochondrial heterogeneity and dysfunction. *J. Biol. Chem.* 280:26185–26192. https://doi.org/10.1074/jbc.M503062200

Cheng, X., X. Zhang, L. Yu, and H. Xu. 2015. Calcium signaling in membrane repair. *In* Seminars in cell & developmental biology. Vol. 45. Amsterdam, Netherlands: Elsevier. 24–31.

Chin, R.M., X. Fu, M.Y. Pai, L. Vergnes, H. Hwang, G. Deng, S. Diep, B. Lomenick, V.S. Meli, G.C. Monsalve, et al. 2014. The metabolite α-ketoglutarate extends lifespan by inhibiting ATP synthase and TOR. *Nature.* 510:397–401. https://doi.org/10.1038/nature13264

Debattisti, V., A. Horn, R. Singh, E.L. Seifert, M.W. Hogarth, D.A. Mazala, K.T. Huang, R. Horvath, J.K. Jaiswal, and G. Hajnóczky. 2019. Dysregulation of mitochondrial Ca2+ uptake and sarcolemma repair underlie muscle weakness and wasting in patients and mice lacking MICU1. *Cell Rep.* 29:1274–1286.e6. https://doi.org/10.1016/j.celrep.2019.09.063

Defour, A., S. Medikayala, J.H. Van der Meulen, M.W. Hogarth, N. Holdreith, A. Malatras, W. Duddy, J. Boehler, K. Nagaraju, and J.K. Jaiswal. 2017. Annexin A2 links poor myofiber repair with inflammation and adipogenic replacement of the injured muscle. *Hum. Mol. Genet.* 26:1979–1991. https://doi.org/10.1093/hmg/ddx065

Defour, A., S.C. Sreetama, and J.K. Jaiswal. 2014. Imaging cell membrane injury and subcellular processes involved in repair. *J. Vis. Exp.* (85):51106. https://doi.org/10.3791/51106

DeKraker, C., L. Goldin-Blais, E. Boucher, and C.A. Mandato. 2019. Dynamics of actin polymerisation during the mammalian single-cell wound healing response. *BMC Res. Notes.* 12:420. https://doi.org/10.1186/s13104-019-4441-7

Demonbreun, A.R., M. Quattrocelli, D.Y. Barefield, M.V. Allen, K.E. Swanson, and E.M. McNally. 2016. An actin-dependent annexin complex mediates plasma membrane repair in muscle. *J. Cell Biol.* 213:705–718. https://doi.org/10.1083/jcb.201512022

Duchen, M.R., A. Leyssens, and M. Crompton. 1998. Transient mitochondrial depolarizations reflect focal sarcoplasmic reticular calcium release in single rat cardiomyocytes. *J. Cell Biol.* 142:975–988. https://doi.org/10.1083/jcb.142.4.975

Favaro, G., V. Romanello, T. Varanita, M. Andrea Desbats, V. Morbidoni, C. Tezze, M. Albiero, M. Canato, G. Gherardi, D. De Stefani, et al. 2019. DRP1-mediated mitochondrial shape controls calcium homeostasis and muscle mass. *Nat. Commun.* 10:2576. https://doi.org/10.1038/s41467-019-10226-9

Frank, S., B. Gaume, E.S. Bergmann-Leitner, W.W. Leitner, E.G. Robert, F. Catez, C.L. Smith, and R.J. Youle. 2001. The role of dynamin-related protein 1, a mediator of mitochondrial fission, in apoptosis. *Dev. Cell.* 1:515–525. https://doi.org/10.1016/S1534-5807(01)00055-7

Friedman, J.R., L.L. Lackner, M. West, J.R. DiBenedetto, J. Nunnari, and G.K. Voeltz. 2011. ER tubules mark sites of mitochondrial division. *Science.* 334:358–362. https://doi.org/10.1126/science.1207385

Glancy, B., L.M. Hartnell, D. Malide, Z.-X. Yu, C.A. Combs, P.S. Connelly, S. Subramaniam, and R.S. Balaban. 2015. Mitochondrial reticulum for cellular energy distribution in muscle. *Nature.* 523:617–620. https://doi.org/10.1038/nature14614

Hamanaka, R.B., and N.S. Chandel. 2010. Mitochondrial reactive oxygen species regulate cellular signaling and dictate biological outcomes. *Trends Biochem. Sci.* 35:505–513. https://doi.org/10.1016/j.tibs.2010.04.002

Han, S.M., H.S. Baig, and M. Hammarlund. 2016. Mitochondria localize to injured axons to support regeneration. *Neuron.* 92:1308–1323. https://doi.org/10.1016/j.neuron.2016.11.025

Horn, A., and J.K. Jaiswal. 2018. Cellular mechanisms and signals that coordinate plasma membrane repair. *Cell. Mol. Life Sci.* 75:3751–3770. https://doi.org/10.1007/s00018-018-2888-7

Horn, A., J.H. Van der Meulen, A. Defour, M. Hogarth, S.C. Sreetama, A. Reed, L. Scheffer, N.S. Chandel, and J.K. Jaiswal. 2017. Mitochondrial redox signaling enables repair of injured skeletal muscle cells. *Sci. Signal.* 10: eaaj1978. https://doi.org/10.1126/scisignal.aaj1978

Jaiswal, J.K., S.P. Lauritzen, L. Scheffer, M. Sakaguchi, J. Bunkenborg, S.M. Simon, T. Kallunki, M. Jäättelä, and J. Nylandsted. 2014. S100A11 is required for efficient plasma membrane repair and survival of invasive cancer cells. *Nat. Commun.* 5:3795. https://doi.org/10.1038/ncomms4795

Kamerkar, S.C., F. Kraus, A.J. Sharpe, T.J. Pucadyil, and M.T. Ryan. 2018. Dynamin-related protein 1 has membrane constricting and severing abilities sufficient for mitochondrial and peroxisomal fission. *Nat. Commun.* 9:5239. https://doi.org/10.1038/s41467-018-07543-w

Katewa, S.D., A. Khanna, and P. Kapahi. 2014. Mitobolites: the elixir of life. *Cell Metab.* 20:8–9. https://doi.org/10.1016/j.cmet.2014.06.013

Kraus, F., and M.T. Ryan. 2017. The constriction and scission machineries involved in mitochondrial fission. *J. Cell Sci.* 130:2953–2960. https://doi.org/10.1242/jcs.199562

Li, N., K. Ragheb, G. Lawler, J. Sturgis, B. Rajwa, J.A. Melendez, and J.P. Robinson. 2003. Mitochondrial complex I inhibitor rotenone induces apoptosis through enhancing mitochondrial reactive oxygen species production. *J. Biol. Chem.* 278:8516–8525. https://doi.org/10.1074/jbc.M210432200

McDade, J.R., A. Archambeau, and D.E. Michele. 2014. Rapid actin-cytoskeleton-dependent recruitment of plasma membrane-derived dysferlin at wounds is critical for muscle membrane repair. *FASEB J.* 28:3660–3670. https://doi.org/10.1096/fj.14-250191

Mishra, P., and D.C. Chan. 2014. Mitochondrial dynamics and inheritance during cell division, development and disease. *Nat. Rev. Mol. Cell Biol.* 15: 634–646. https://doi.org/10.1038/nrm3877

Motulsky, H.J., and R.E. Brown. 2006. Detecting outliers when fitting data with nonlinear regression - a new method based on robust nonlinear regression and the false discovery rate. *BMC Bioinformatics.* 7:123. https://doi.org/10.1186/1471-2105-7-123

Murley, A., and J. Nunnari. 2016. The emerging network of mitochondria-organelle contacts. *Mol. Cell.* 61:648–653. https://doi.org/10.1016/j.molcel.2016.01.031

Otera, H., N. Miyata, O. Kuge, and K. Mihara. 2016. Drp1-dependent mitochondrial fission via MiD49/51 is essential for apoptotic cristae remodeling. *J. Cell Biol.* 212:531–544. https://doi.org/10.1083/jcb.201508099

Pagliuso, A., P. Cossart, and F. Stavru. 2018. The ever-growing complexity of the mitochondrial fission machinery. *Cell. Mol. Life Sci.* 75:355–374. https://doi.org/10.1007/s00018-017-2603-0

Palmer, C.S., L.D. Osellame, D. Laine, O.S. Koutsopoulos, A.E. Frazier, and M.T. Ryan. 2011. MiD49 and MiD51, new components of the mitochondrial fission machinery. *EMBO Rep.* 12:565–573. https://doi.org/10.1038/embor.2011.54

Pertz, O., L. Hodgson, R.L. Klemke, and K.M. Hahn. 2006. Spatiotemporal dynamics of RhoA activity in migrating cells. *Nature.* 440:1069–1072. https://doi.org/10.1038/nature04665

Riedl, J., K.C. Flynn, A. Raducanu, F. Gärtner, G. Beck, M. Bösl, F. Bradke, S. Massberg, A. Aszodi, M. Sixt, and R. Wedlich-Söldner. 2010. Lifeact mice for studying F-actin dynamics. *Nat. Methods.* 7:168–169. https://doi.org/10.1038/nmeth0310-168

Salka, K., S. Bhuvanendran, K. Wilson, P. Bozidis, M. Mehta, K. Rainey, H. Sesaki, G.H. Patterson, J.K. Jaiswal, and A.M. Colberg-Poley. 2017. Superresolution imaging identifies that conventional trafficking pathways are not essential for endoplasmic reticulum to outer mitochondrial membrane protein transport. *Sci. Rep.* 7:16. https://doi.org/10.1038/s41598-017-00039-5

Sharma, N., S. Medikayala, A. Defour, S. Rayavarapu, K.J. Brown, Y. Hathout, and J.K. Jaiswal. 2012. Use of quantitative membrane proteomics identifies a novel role of mitochondria in healing injured muscles. *J. Biol. Chem.* 287:30455–30467. https://doi.org/10.1074/jbc.M112.354415

Steinhardt, R.A., G. Bi, and J.M. Alderton. 1994. Cell membrane resealing by a vesicular mechanism similar to neurotransmitter release. *Science.* 263: 390–393. https://doi.org/10.1126/science.7904084

Szabadkai, G., A.M. Simoni, K. Bianchi, D. De Stefani, S. Leo, M. Wieckowski, and R. Rizzuto. 2006. Mitochondrial dynamics and Ca2+ signaling. *Biochim. Biophys. Acta.* 1763:442–449.

Tilokani, L., S. Nagashima, V. Paupe, and J. Prudent. 2018. Mitochondrial dynamics: overview of molecular mechanisms. *Essays Biochem.* 62: 341–360. https://doi.org/10.1042/EBC20170104

Vila, M.C., S. Rayavarapu, M.W. Hogarth, J.H. Van der Meulen, A. Horn, A. Defour, S. Takeda, K.J. Brown, Y. Hathout, K. Nagaraju, and J.K. Jaiswal. 2017. Mitochondria mediate cell membrane repair and contribute to Duchenne muscular dystrophy. *Cell Death Differ.* 24:330–342. https://doi.org/10.1038/cdd.2016.127

Wakabayashi, J., Z. Zhang, N. Wakabayashi, Y. Tamura, M. Fukaya, T.W. Kensler, M. Iijima, and H. Sesaki. 2009. The dynamin-related GTPase Drp1 is required for embryonic and brain development in mice. *J. Cell Biol.* 186:805–816. https://doi.org/10.1083/jcb.200903065

Westermann, B. 2012. Bioenergetic role of mitochondrial fusion and fission. *Biochim. Biophys. Acta.* 1817:1833–1838. https://doi.org/10.1016/j.bbabio.2012.02.033

Wu, A.H., and M.B. Perryman. 1992. Clinical applications of muscle enzymes and proteins. *Curr. Opin. Rheumatol.* 4:815–820.

Wu, J., L. Liu, T. Matsuda, Y. Zhao, A. Rebane, M. Drobizhev, Y.-F. Chang, S. Araki, Y. Arai, K. March, et al. 2013. Improved orange and red Ca^{2}± indicators and photophysical considerations for optogenetic applications. *ACS Chem. Neurosci.* 4:963–972. https://doi.org/10.1021/cn400012b

Xu, S., and A.D. Chisholm. 2014. C. elegans epidermal wounding induces a mitochondrial ROS burst that promotes wound repair. *Dev. Cell.* 31: 48–60. https://doi.org/10.1016/j.devcel.2014.08.002

Youle, R.J., and A.M. van der Bliek. 2012. Mitochondrial fission, fusion, and stress. *Science.* 337:1062–1065. https://doi.org/10.1126/science.1219855

Yun, J., and T. Finkel. 2014. Mitohormesis. *Cell Metab.* 19:757–766. https://doi.org/10.1016/j.cmet.2014.01.011

Zhou, B., P. Yu, M.-Y. Lin, T. Sun, Y. Chen, and Z.-H. Sheng. 2016. Facilitation of axon regeneration by enhancing mitochondrial transport and rescuing energy deficits. *J. Cell Biol.* 214:103–119. https://doi.org/10.1083/jcb.201605101

Supplemental material

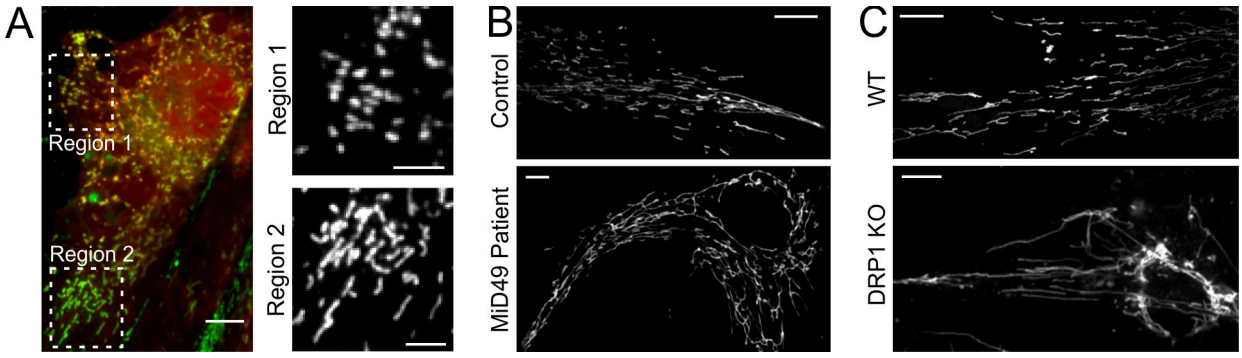

Figure S1. **Mitochondrial morphology after injury and genetic KO of fission regulators MiD49 and Drp1. (A)** Images showing WT MEF injured by glass bead. Injured cells are marked by presence of TRITC-dextran (red). Mitochondria are marked by MitoTracker Green (green). Magnified regions show area of mitochondrial fragmentation near injury site (Region 1) and area containing tubular mitochondria distal to injury site (Region 2). **(B)** Images showing mitochondria in healthy control and MiD49 patient fibroblasts. **(C)** Images showing mitochondrial shape in WT and DRP1 KO MEFs. In all cases, mitochondria are marked by MitoTracker Green. Scale bar = 10 µm or 5 µm (A, zoom).

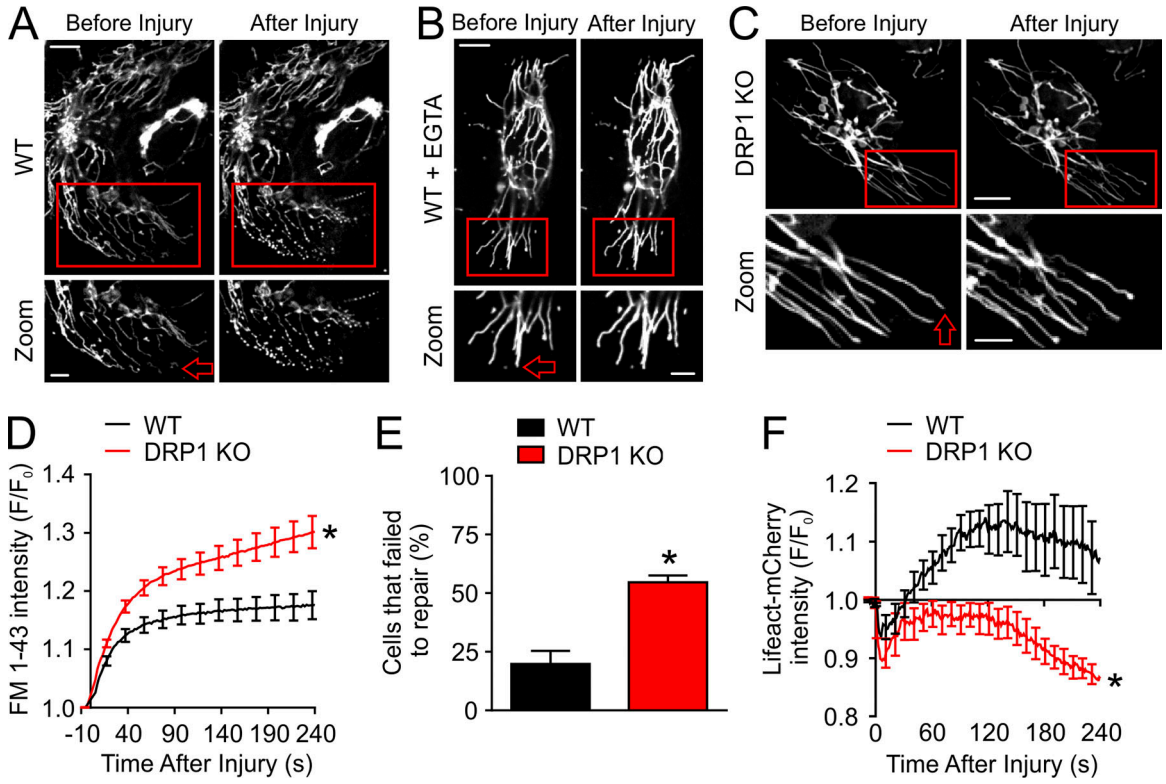

Figure S2. **Injury-triggered mitochondrial fragmentation is conserved in HeLa cells. (A–C)** Images showing mitochondrial shape in response to PM injury in WT (A), EGTA-treated WT (B), and DRP1 KO (C) HeLa cells. In all cases, mitochondria are marked by TOM20, a structural protein of the OMM. Arrows mark the site of injury. Boxes indicate the area of zoom shown below. Scale bar = 10 µm (whole cell) and 5 µm (zoom). **(D)** Plot showing FM 1-43 dye intensity after injury in WT (n = 31) and DRP1 KO (n = 44) HeLa cells. **(E)** Plot showing percentage of cells that failed to repair in independent experiments (n = 3). **(F)** Plot showing Lifeact-mCherry intensity after PM injury in WT (n = 5) and DRP1 KO (n = 7) HeLa cells. *, $P < 0.05$ by unpaired t test. Error bars represent SEM.

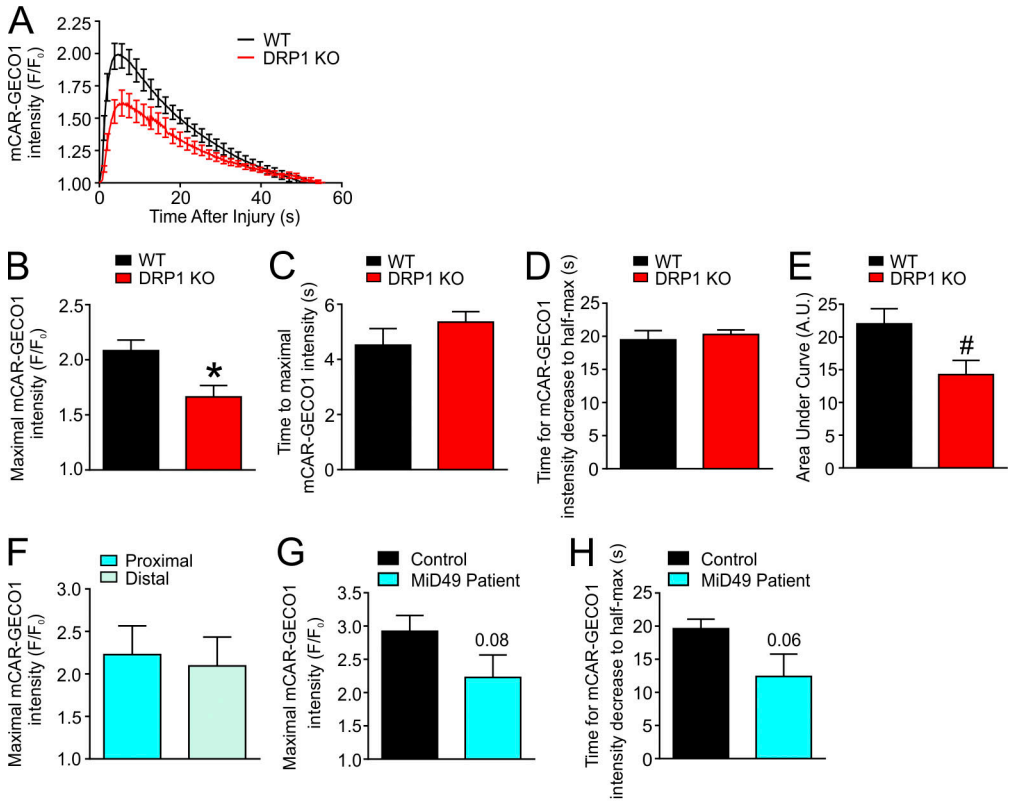

Figure S3. **Mitochondrial calcium uptake after PM injury in DRP1 KO and MiD49 patient cells. (A)** Plot showing mCAR-GECO1 intensity after PM injury in WT (n = 12) and DRP1 KO MEFs (n = 14 cells). Calcium uptake was quantified over the entire cell, including both injury proximal and distal mitochondria. **(B–E)** Quantification of mitochondrial calcium uptake in WT and DRP1 KO cells after injury showing peak mitochondrial calcium (B), time to reach peak mitochondrial calcium (C), time for mitochondrial calcium to decrease to half peak (D), and area under the curve (E), illustrating mitochondrial calcium load from time of injury until calcium returned to baseline (n = 12 WT and 14 DRP1 KO cells for each). **(F)** Peak calcium uptake in injury-proximal and distal mitochondria of MiD49 patient cells (n = 6 cells). **(G)** Peak calcium uptake in injury-proximal mitochondria from healthy control and MiD49 patient cells (n = 9 control and 6 patient cells). **(H)** Quantification of time for calcium to reach half peak in control and MiD49 patient cells (n = 9 control and 6 patient cells). *, P < 0.05 by unpaired t test. #, P < 0.05 by Mann–Whitney U test. Error bars represent SEM.

Video 1. **PM injury causes rapid fragmentation of mitochondria.** WT MEF labeled with MitoTracker Green was focally injured and imaged at 2 frames/s. The video shows the portion of the cell proximal to the injury site, demonstrating that injury-induced mitochondrial fragmentation occurs within seconds after injury.

Video 2. **Injury-triggered mitochondrial fragmentation in a healthy human fibroblast.** Primary human fibroblast labeled with MitoTracker Green was focally injured and imaged at 2 frames/s. The video shows the portion of the cell proximal to the injury site, demonstrating that injury-induced mitochondrial fragmentation occurs within seconds after injury.

Video 3. **MiD49 is required for injury-triggered mitochondrial fragmentation.** Primary fibroblast from Mid49 patient labeled with MitoTracker Green was focally injured and imaged at 2 frames/s. The video shows the portion of the cell proximal to the injury site, demonstrating that injury fails to induce mitochondrial fragmentation.

Video 4. **Drp1 recruitment to injury-proximal mitochondria following PM injury.** Mitochondria in WT MEF were colabeled by transient expression of TOM20-YFP (green) and Drp1-mCherry (red). The video shows the portion of the cell proximal to the injury site imaged every 2 s, demonstrating rapid, focal PM injury-triggered accumulation of Drp1 on the fragmenting mitochondria.

Video 5. **Drp1 is required for injury-triggered mitochondrial fragmentation.** DRP1 KO MEF was labeled with MitoTracker Green, focally injured, and imaged at 1 frame/s. The video shows the portion of the cell proximal to the injury site, demonstrating failure of the mitochondria to fragment in response to PM injury.